AIAA Guidance, Navigation, and Control Conference
13 - 16 August 2012, Minneapolis, Minnesota

AIAA 2012-4605

A Novel Solution for Overflight and Surveying of a Collaborative Target with Fixed Wing UAV

Niki Regina* and Matteo Zanzi †
University of Bologna, Forli', FC, 47100, Italy

This study presents a new guidance law for a fixed-wing Unmanned Aerial Vehicle (UAV) with surveillance and/or tracking purposes. In particular the algorithm ensures a continue overflying of the target whether it is fixed or when it moves. Particular attention is paid to the definition of the guidance specifications in order to derive a suitable guidance law capable to fulfill the requirements under tight constrains like the constancy of airspeed and bounded lateral accelerations. Stability proof of the proposed guidance law, together with parameter definition criteria have been developed. An assessment of the performances of the presented law is given by means of software simulations and hardware-in-the-loop tests.

Nomenclature

R	Horizontal Distance between Pursuer and Target
$\vec{R}$	Pursuer and Target Vector in the Horizontal Plane
ψ	UAV Heading Angle
χ	UAV Course Angle
χ_T	Target Course Angle
χ_W	Wind Course Angle
x, y	UAV Horizontal Position Coordinates
x_T, y_T	Target Horizontal Position Coordinates
σ	Target-Pursuer LOS Angle
V	UAV Airspeed, m/s
$\vec{V}$	UAV Airspeed Vector, m/s
V_G	UAV Ground Speed, m/s
V_T	Target Speed, m/s
W_x, W_y	Wind Velocities Along North and East Axes
ϕ	UAV Bank Angle
θ	UAV Pitch Angle
ρ	Air Density
D	Drag force, N
C_{D_0}	zero-lift drag coefficient
C	Gain of the proposed Guidance Law
g	gravitational acceleration
$\bar{K}$	induced drag factor
m	Mass, Kg
h	height, m
S	Wing span, m^2
E	Efficiency
Subscript	
i	Variable number

*Assistant Researcher, Advanced Research Center on Electronic Systems, ARCES, **niki.regina2@unibo.it**
†Assistant Professor, Department of Electronics, Computer Science and Systems, DEIS, **matteo.zanzi@unibo.it**

I. Introduction

During the past decade, a growth in UAV technologies has made possible different tasks. One of the most important is the capability of the air vehicle to track a moving ground target through the use of a gimbaled camera. Usually a gimbal operator on the ground selects a target of interest using a joystick that moves the gimbaled camera. Once the target is selected the UAV and camera automatically track the target. This kind of system also performs a real time estimation of the target's velocity using UAV-gimbal telemetry data and the extracted target position on the image plane. Information about this scientific theme is available in Ref.[12] and in Ref.[3] where similar approaches are presented.

In this paper the target is assumed to be friendly and its position known by the pursuer guidance system. The target position is assumed to be determined by itself and transmitted via data-link to the flying pursuer. It is an aim of the pursuer UAV to autonomously follow the target during its maneuvers, by avoiding to go too far away from it, as well as if the UAV is kept in a virtual leash by the target.

The aim of this paper is to develop a guidance law able to ensure a continuous loitering over the target when it is keeping still and to create a bounded trajectory around the position of the target when it moves.

In order to create a guidance algorithm two main different scenarios are considered in literature:

1. The UAV flies autonomously along a predefined trajectory created around the fixed position of the target;

2. The UAV creates by itself a trajectory around the moving target.

With reference to the first scenario, the tracking problem is transformed to a path-following problem. A representative guidance law design technique recently presented in literature is the Lyapunov vector field (see Ref.[45]). An inner feedback control loop is assumed to ensure the vehicle tracks the vector field by actuating the aircraft control surfaces in order to produce aerodynamics moments to achieve the desired vehicle attitude and altitude hold mode. The direction and the magnitude of the computed vector field velocity are transformed by the guidance outer loop into heading commands, suitable to assure the maneuvers of the UAV to be consistent to its flight performances in terms of minimum required air-speed and maximum turn-rate. In Ref.[6] a vector field for continuous live sensing is created through the use of a particular figure known as Lemniscate. Within the first scenario also the design techniques based on a imaginary point moving along the predefined trajectories must be included. This point is called pseudo-target or ghost-target or virtual-target. This approach is used in Ref.[78] and Ref.[9] (here a 3D tracking is considered) where a guidance method for tracking straight line and curved path is presented. This guidance law is similar to a pure-pursuit guidance as described in Ref.[10]

An hybrid solution is presented in Ref.[1112] and Ref.[13] In these papers an oscillatory ghost-target is created around the moving or fixed position of the target. Consequently the UAV is forced to track the factious target by different guidance laws. This approach is definitely an improvement respect to the approaches cited until now although neither of them consider the problem of out-of-frame target images.

With reference to the second scenario, the guidance laws presented in Ref.[14] are able to track a moving target within a fixed horizontal range chosen by the operator. Besides, it is able to track the target even if it is out-of-frame. One limit of this guidance law is when the horizontal range is equal to zero due to disturbances, for instance. In this case the commanded acceleration is unbounded.

The guidance law presented in Ref.[15] solves this problem. It can be seen in the simulations that, even if the distance happens to be equal to zero, the UAV stabilizes itself on a circle whose radius meets the UAV dynamics (see Ref.[16])

In this paper, using an approach similar to the last two cited articles, a new non-linear two dimension (2D) guidance law is presented. It generates petal-like trajectories along an horizontal plane at an established flight altitude, centered around a ground target, that ensures a continuous loitering over the target whether it keeps still or moves. The main features of the proposed law are twofold: its simplicity and adaptability to various tracking scenarios. In fact, according to this law, the UAV does not follow a path with a predefined shape created around the target; rather, it creates a trajectory whose points are computed in real time by the UAV itself depending on target available position and velocity data.

Similarly as in most flight applications, a separate inner and outer feedback-loop control approach is assumed in this work. This because of its simplicity and the availability of good autopilots for attitude stabilization and altitude hold. The outer guidance loop transforms the lateral acceleration computed by the guidance law into heading commands. The guidance law is suitable to guarantee the maneuvers of the

UAV to be consistent to its flight performances in terms of minimum required air-speed and maximum turn-rate. The computation of the guidance law requires the knowledge of the UAV/Target Line-Of-Sight (LOS) and the LOS rate. Moreover, a few parameters have to be chosen and tuned according to the UAV flight performances and mission requirements (related to target over-flying repetition rate).

The significance of the proposed guidance algorithm respect to the existing ones consists in the fact that no fuel, time or distance-based cost function are minimized by the control law; instead, it allows a UAV for the continuous overflight of a target without the need of the design of a predefined trajectory.

Results are shown by providing simulations and tests. Numerical simulations of different tracking scenarios are proposed in order to show the behavior of the law, also taking into account wind effect. Besides, tests with a well known X-Plane 6DoF simulator are accomplished in order to evaluate the realistic behavior of the implemented guidance law on an existing aerial vehicle.

The paper is organized as follows. Section 2 describes the mathematical model of the target tracking problem. Section 3 presents the proposed guidance law and its main features. A stability analysis is given here. Section 4 is dedicated to the target velocity estimation. In section 5 some simulation results in order to evaluate the effectiveness of the law. Section 6 implements the proposed guidance law on X-Plane 6DoF simulator.

II. Model of the target-tracking problem

In order to develop a guidance law for a fixed-wing UAV that tracks a ground target, some assumptions have been stated in this work. Firstly, the motion of the UAV is considered at constant altitude, herein the problem can be considered a two dimensional (2D) tracking problem. Moreover, the airspeed of the UAV is assumed to be constant in order to provide the necessary lift to hold the altitude as much as possible. Besides, the control input of the airplane is the lateral acceleration caused by aileron deflections and the lateral acceleration in its turn gives raise a heading change.
Herein the UAV has been modeled as a mass-point moving on a horizontal plane according to the following mathematical model:

$$\begin{cases} \dot{x} = V\cos(\psi) + W_x \\ \dot{y} = V\sin(\psi) + W_y \\ \dot{\psi} = \frac{a_n}{V} \end{cases} \tag{1}$$

where $[x, \ y, \ \psi]^T$ is the state vector of the UAV model and the state variables represent the two cartesian position coordinates along a North-East reference frame and the heading angle, respectively. W_x and W_y are the wind velocity components. The angle ψ is positive in an anti-clockwise sense and it represents the angle between the x (North) axis and the longitudinal UAV axis; this, in turn, coincides with the direction of the UAV airspeed vector $\vec{V}$ because no sideslip angle is considered. V is the norm of $\vec{V}$. a_n is the single input signal of the model and represents the value of lateral acceleration. No longitudinal acceleration respect to the air flow is considered because $\dot{V} = 0$. As told before, the effect of the lateral acceleration is to cause a change in the rate of turn while leaving the airspeed unchanged.

In case of no wind the heading angle coincides with the course angle χ, i.e. the ground-track velocity-vector angle respect to the North direction.

In a target tracking problem is interesting to analyze the evolution of the geometry of the relative target-pursuer motion rather than the single position of the mass points. In particular, according to Ref.[10] , the dynamic behavior of the projection of the relative target-pursuer distance on the horizontal plane, R, together with the Line-Of-Sight (LOS) angle σ, is described by the following dynamic model:

$$\begin{cases} \dot{R} = V_T\cos(\sigma - \chi_T) - V_G\cos(\sigma - \chi) \\ R\dot{\sigma} = -V_T\sin(\sigma - \chi_T) + V_G\sin(\sigma - \chi) \end{cases} \tag{2}$$

where V_T and χ_T are the target speed and course angle, respectively, while V_G is the UAV ground speed, R is the target-UAV distance.

Of course there is a relationship among models (1) and (2). In fact, $V_G = \sqrt{\dot{x}^2 + \dot{y}^2}$ and $R = \sqrt{(x_T - x)^2 + (y_T - y)^2}$, with $[x_T, y_T]^T$ the position coordinates of the target; moreover, $\tan\chi = \dot{y}/\dot{x}$.

A representation of the involved variables is given in Fig. 1.

As a consequence of the above discussion is $V_G = V_G(\psi, W_x, W_y)$ where

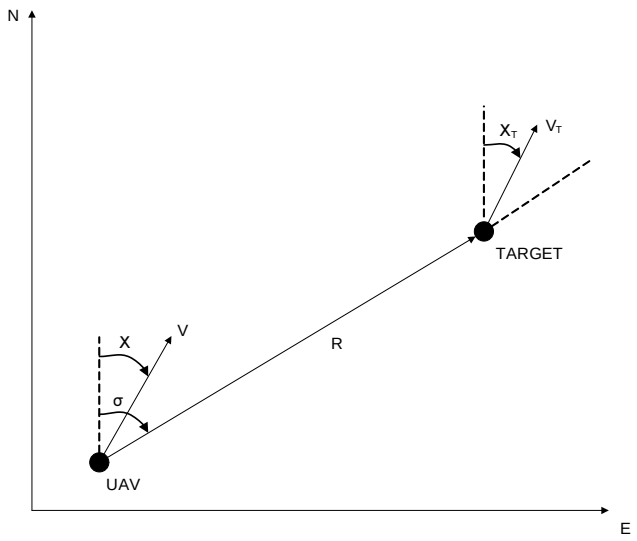

Figure 1. Target-Pursuer Relative Geometry

$$V_G(\psi, W_x, W_y) := \sqrt{(V\cos(\psi) + W_x)^2 + (V\sin(\psi) + W_y)^2} \tag{3}$$

and, by defining

$$g(\psi, W_x, W_y) := \arctan 2\left(V\sin(\psi) + W_y, V\cos(\psi) + W_x\right) \tag{4}$$

where $z = \arctan 2\,(b, a)$ is the usual four-quadrant arc tangent function such that $\tan\left(\arctan 2(b, a)\right) = \frac{b}{a}$, it is

$$\chi = g(\psi, W_x, W_y) \tag{5}$$

For the discussion in the next section it is also worth noting that

$$g\left(\psi, 0, 0\right) = \psi \tag{6}$$

and

$$V_G(\psi, 0, 0) = V \tag{7}$$

Finally, a mathematical model suitable for the UAV-Target tracking problem studied in this work is obtained by using eq. (1), eq. (2), eq. (3) and eq. (5) that yield to:

$$\begin{cases} \dot{R} = V_T\cos(\sigma - \chi_T) - V_G(\psi, W_x, W_y)\cos(\sigma - g(\psi, W_x, W_y)) \\ R\dot{\sigma} = -V_T\sin(\sigma - \chi_T) + V_G(\psi, W_x, W_y)\sin(\sigma - g(\psi, W_x, W_y)) \\ \dot{\psi} = \frac{a_n}{V} \end{cases} \tag{8}$$

Model (8) is a third order dynamic model where $[R,\ \ \sigma,\ \ \psi]^T$ is the state vector, a_n is the input, V_T and χ_T are time varying parameters, V, W_x and W_y are constant parameters.

III. Proposed Guidance Law

A. Motivation of The Guidance Law Structure

In this paper it is assumed that the position and velocity of the target are known by the UAV guidance system. In Ref.[17] and Ref.[18] a description of typical sensors useful for this aim are given. Then, the state of

system (8) is observable. Moreover, the wind velocity is assumed to be known. According to this hypothesis, in eq. (8) V_T, χ_T, W_x and W_y can be considered as measurable parameters.

The requirements of the problem of guidance here considered can be summarized as follows.

The UAV has to track the target continuously. In order to do this, its airspeed is not lower than the target ground speed; rather, its airspeed is almost always greater then that of the target. As a consequence of this, the UAV usually reaches and overflies the target: hence a maneuver for turning back on the target after an overtaking is necessary.

The turning back has to be accomplished through turn rates compliant with the mechanical characteristics of the aircraft, and lateral accelerations required for these maneuvers have to be bounded. As previously recalled, during all the tracking maneuvers the airspeed of the UAV has to be maintained unchanged.

In order to derive a guidance law fulfilling the stated requirements, it can be designed according to the following specifications.

At first, the guidance law has to act on the lateral acceleration a_n, the only one controllable input of the system. The guidance law has to provide bounded signals.

Moreover, the guidance law has to steer the UAV to head the target when the UAV is approaching it. In this, the guidance law has to behave as a typical proportional navigation guidance. In particular, the guidance law has to be a function of the angle among the LOS and UAV ground velocity vector, i.e. $\sigma - \chi$.

Nevertheless, during overflying and after, the guidance law needs to give the UAV time sufficient to move away the target enough in order to gain the necessary range to be able to:

- turn back with a maneuver not so strong as to require an excessive lateral acceleration, that is to let admissible curvature radii;
- come back by heading toward the target avoiding to remain trapped on a loitering circle with a fixed radius around the target itself. This specification is necessary to avoid behaviors that imply steady limit cycles as in[15].

The proposed guidance law has therefore the following form:

$$a_n = K_1(R, \dot{R}) \arctan(K_2(\sigma - \chi)) \tag{9}$$

where

- $K_1() : \mathbb{R}^+ \times \mathbb{R} \to \mathbb{R}^+$;
- K_2 is considered positive in the interval]0,1]

In particular, function K_1 acts as a state-dependent gain that modulates the strength of the lateral acceleration provided by the guidance law. It acts according to the following criterion: when the UAV is going away after overflying the target but is yet near it within a circular area specified by a predefined radius R_0, the gain must be at its lowest value; otherwise it reaches its maximum value.

While it is possible to find out a smooth version of gain K_1, a discrete behavior has been selected in this work in order to evaluate the overall performances of the guidance law. Hence, the gain function is specified in table 1.

Table 1. Gain Selection for the Guidance Mode

	$R < R_0$	$R \geq R_0$
$\dot{R} < 0$	C	C
$\dot{R} \geq 0$	0	C

with $C \in \mathbb{R}^+$. Value of C, K_2 and R_0 can be selected by a tuning phase, even if an analytical approach is proposed in the next section.

B. Advantages of The Proposed Guidance Law

In order to evaluate the usefulness of the proposed guidance law, a comparison with the one presented in Ref.[16] is made. The analysis is based on the work of Ref.[19] where basic patterns of unmanned aerial vehicle are proposed and analyzed to maximize the "seeability" and or to minimize power consumptions.

In the two subsequent examples the ScanEagle UAV following UAV parameters are used reflective of the :

- E_{max}=14;
- C_{D_0}=0.04;
- $S = 1.0110\ [m^2]$;
- $V = 60.9756\ [m/s]$;
- $h = 1000$ [m];
- $m = 18$ [kg]

The normalized power $\bar{P}$ is defined as the power divided by the weight. Hence it results:

$$\bar{P} = \frac{DV}{mg} = \bar{\rho}V\left(C_{D_0} + \bar{K}C_L^2\right) = \bar{\rho}C_{D_0}V + \frac{\bar{K}}{\bar{\rho}}\frac{1}{\cos^2(\phi)} \tag{10}$$

where

$$\bar{\rho} = \frac{\rho S V^2}{2\,(mg)}$$

and

$$\bar{K} = \frac{1}{4E_{max}^2 C_{D_0}}$$

Two different simulations are now presented. In the first one the target is considered fixed at the origin of a North-East reference frame. The initial position of the UAV is at (2600,2600), with north initial heading. The desired radius R_0 is chosen to be 500 [m].

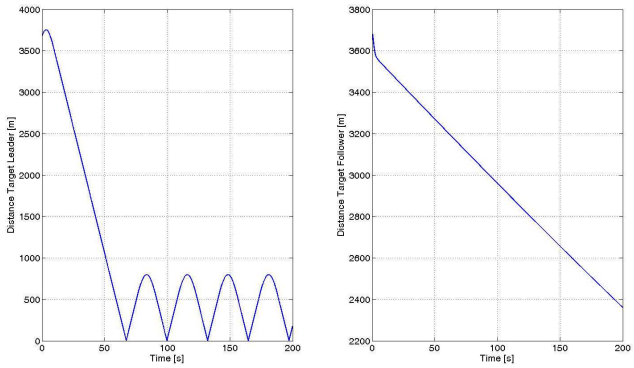

Figure 2. Pursuer-Target Distance Comparison

In Fig. 2 it can be seen how the new proposed guidance law (left) is faster to approach the target than the guidance law proposed by Kaminer and all (right). In fact the time mean distance decreases from 2965 [m] to 989 [m]. Moreover, by observing Fig. 3, even if the the distance decreases, the mean power consumption [Watt/Newton] remains unchanged and, consequently, the endurance (the scale of the two figures is different).

The same conclusion can be deduced if the target is moving as show in the next figures (the proposed law is on the left of the figures).

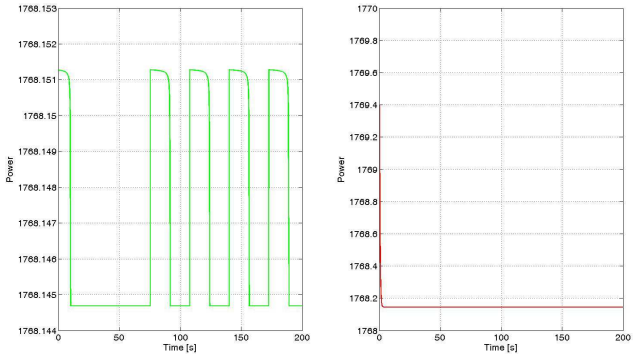

Figure 3. Power Comparison

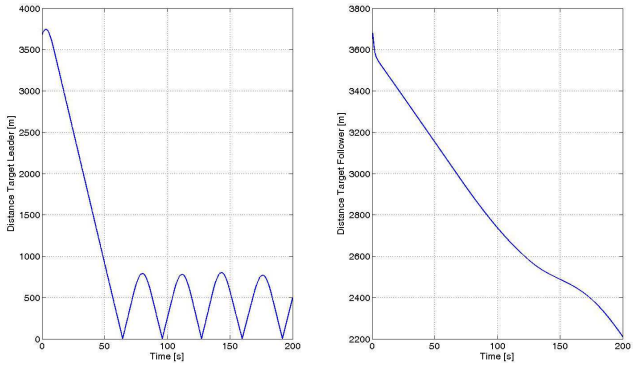

Figure 4. Distance Comparison with Moving Target

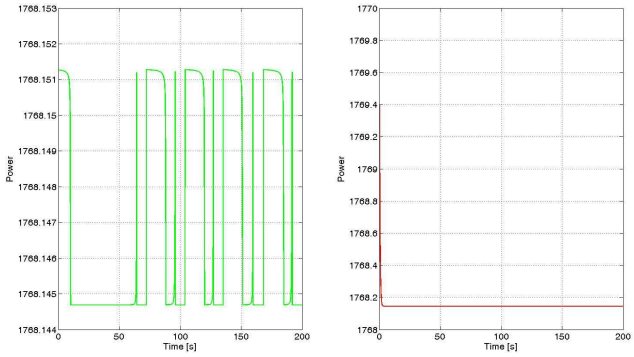

Figure 5. Power Comparison with Moving Target

IV. Proof of Stability

In order to demonstrate the stability of the proposed guidance law (9) and to give an analytical method for the choice of the gains, the tracking problem has been dealt with according to two cases:

1. fixed target position and no wind effects;
2. moving target with no wind effects.

A. Fixed Target

Starting from eq. (8), and considering a fixed position for the target ($V_T = 0$) with no wind effect ($W = 0$) the mathematical model of the Pursuer-Target (P-T) relative motion becomes:

$$\begin{cases} \dot{R} = -V\cos(\sigma - \psi) \\ R\dot{\sigma} = V\sin(\sigma - \psi) \\ \dot{\psi} = \frac{K_1(R,\dot{R})\arctan(K_2(\sigma-\psi))}{V} \end{cases} \tag{11}$$

It is possible to define a new state variable $\alpha = \sigma - \psi$ in order to arrive to a second order system:

$$\begin{cases} \dot{R} = -V\cos(\alpha) \\ \dot{\alpha} = \frac{V\sin(\alpha)}{R} - \frac{K_1(R,\dot{R})\arctan(K_2\alpha)}{V} \end{cases} \tag{12}$$

As known from Ref.[20] it could be possible to construct the phase portrait of (12). The first step is to find all the equilibrium points and to determine their stability properties.

$$\begin{cases} \cos(\alpha) = 0 \\ \frac{V\sin(\alpha)}{R} - \frac{K_1(R,0)\arctan(K_2\alpha)}{V} = 0 \end{cases} \tag{13}$$

From the first of (13) it results that in the phase plane (α, R) the abscissa coordinate of the equilibrium points is $\alpha = \pm\frac{\pi}{2}$. Due to the nonlinear gain K_1 and the second line of table 1, the same phase plane can be split into two different regions:

1. with $R < R_0$;
2. with $R \geq R_0$.

In the first region the value of K_1 is equal to zero (when $\dot{R} = 0$) and no equilibrium point exists in this region.

In the second region there are two equilibrium points $P_1 = (\alpha_1, R_e)$ and $P_2 = (\alpha_2, R_e)$ where

$$\begin{cases} \alpha_1 = -\frac{\pi}{2} \\ \alpha_2 = \frac{\pi}{2} \\ R_e = \frac{V^2}{C\arctan(K_2\frac{\pi}{2})} \end{cases} \tag{14}$$

under the condition that

$$R_e \geq R_0 \tag{15}$$

In particular in the phase plane the two equilibrium points are at the intersection between the two straight lines $\alpha = -\frac{\pi}{2}$, $\alpha = \frac{\pi}{2}$ and the curve $R = \frac{V^2\sin\alpha}{C\arctan(K_2\alpha)}$.

It must be highlighted that the proposed guidance law (9) is bounded and is

$$|a_n| < C\frac{\pi}{2} \tag{16}$$

Moreover, from eq. (14-15) it is also possible to derive a condition for K_2 in order to have an equilibrium point.

In fact:

$$K_2 = \frac{2}{\pi}\tan(\frac{V^2}{CR_e}) \leq \frac{2}{\pi}\tan(\frac{V^2}{CR_0}) \tag{17}$$

Remark

In order to have a reference value for the maximum lateral acceleration, it is worth noting that: by considering a plane flying along constant rate turn maneuver, it experiences a lateral acceleration given by $\frac{V^2}{R}$ *where* R *is the turn radius. Hence, the maximum value for the lateral acceleration can be chosen from this expression by selecting a suitable minimum value* R_{min} *for* R*. That is:*

$$|a_n|_{max} = \frac{V^2}{R_{min}} \tag{18}$$

Moreover, by considering the well known flight mechanical equation for the coordinate turn [Ref.[21]*] is*

$$g\tan(\phi) = \frac{V^2}{R} \tag{19}$$

where ϕ *is the bank angle. By selecting a maximum bank angle value* $\phi_{max} = |\phi|_{max}$ *for a chosen UAV, it is possible to compute an expression for the minimum value of the turn radius* R_{min}*:*

$$R_{min} = \frac{V^2}{g\tan(\phi_{max})} \tag{20}$$

Hence, by posing $|a_n|_{max} = C\frac{\pi}{2}$ *the gain of the guidance law results:*

$$C = \frac{2g\tan(\phi_{max})}{\pi} = \frac{2V^2}{\pi R_{min}} \tag{21}$$

As it has been discussed in the previous sections, the aim of this guidance law is to ensure with a fixed position of the target a continuous over-loiter. For this reason the equilibrium points which would drive the UAV on a circular trajectory must be avoided. To this aim, from (17) and the considerations presented in the remark, the following condition is sufficient to hold:

$$K_2 > \frac{2}{\pi}\tan(\frac{\pi V^2}{4R_0 g\tan(\phi_{max})}) \tag{22}$$

The arrows in Fig. 6 show the components of the vector field associated to the system, $\dot{R}$ and $\dot{\alpha}$, in the phase portrait. The horizontal line represents the value of R_0 while the continuous line is computed by numerically solving $R = \frac{V^2\sin(\alpha)}{C\arctan(K_2\alpha)}$ which corresponds to $\dot{\alpha} = 0$. This line lies under the predefined radius R_0 due to the conditions for the equilibrium points.

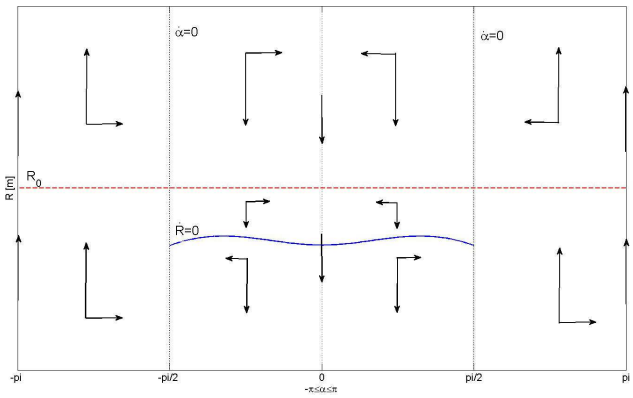

Figure 6. Vector field diagram

From Fig. 6 it is possible to derive an upper bound for the maximum reached distance R starting from any initial condition. In fact, it can be seen that the distance increases only into the two regions: 1)

$-\pi < \alpha < -\frac{\pi}{2}$, 2) $\frac{\pi}{2} < \alpha < \pi$. The slope of vector field is described by eq. (23) and it is plotted in Fig. 7 only for the first region:

$$\frac{dR}{d\alpha} = \frac{\dot{R}}{\dot{\alpha}} = -\frac{V^2 R\cos(\alpha)}{V^2\sin(\alpha) - CR\arctan(K_2\alpha)} \tag{23}$$

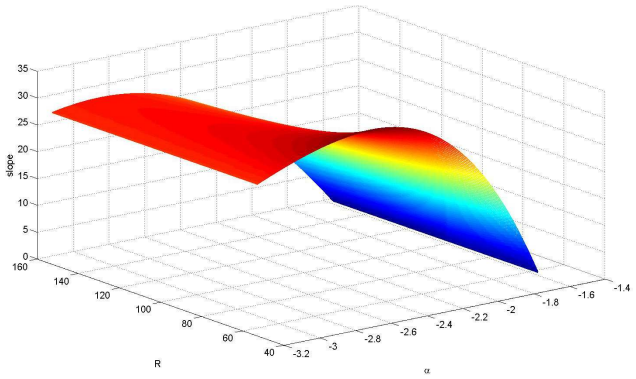

Figure 7. Slope of the Vector Field

By assigning a fixed value to α in this first region it can be easily demonstrated that the partial derivative $\frac{\partial\left(\frac{dR}{d\alpha}\right)}{\partial R}$ is negative; this means that with a fixed α the slope of the vector field is decreasing as R increases.

It can also be found the value $\bar{\alpha}$ of α corresponding to the maximum slope of the vector field, having R as a parameter; $\bar{\alpha}$ is obtained by numerically solving the following equation:

$$V^2 R\left(V^2 - RC\left(\sin(\bar{\alpha})\arctan(K_2\bar{\alpha}) + \frac{K_2\cos(\bar{\alpha})}{1+(K_2\bar{\alpha})^2}\right)\right) = 0 \tag{24}$$

Once $\bar{\alpha}$ has been detected numerically, it can be substituted into eq. (23) in order to find the maximum slope value s_{max} of the vector field in this region for a stated R.

Hence, starting from a generic point (α_i, R_i) with $\alpha_i \in [-\pi, -\frac{\pi}{2}]$ and using the following linear equation,

$$R_{(-\frac{\pi}{2})} = R_i - s_{max}\left(\frac{\pi}{2} + \alpha_i\right) \tag{25}$$

it is possible to define $R_{(-\frac{\pi}{2})}$ as an upper bound for the phase plane as it is shown in Fig. 8 .

Now, considering the bounded subset $M = \left\{(R,\alpha) : R \le R_{-\frac{\pi}{2}}\right\}$ the Poincaré-Bendixson criterion (see Ref.[20]) is satisfied and a periodic orbit exists inside the subset. In particular Fig. 9 shows how the periodic orbit is reached starting from two different initial conditions. In particular it must be highlighted that there is only one isolated periodic orbit which can be called limit cycle. As it can be seen all the trajectories inside the bounded set tend towards a limit cycle.

In order to demonstrate the stability of the proposed guidance law when the target is moving, an alternative analytical stability demonstration for a fixed target has to be given. For this aim a change of variable is made: $\hat{R} = R/\bar{R}$ where $\bar{R}$ is a constant value greater than R_0. In this way, $\dot{\hat{R}} = \dot{R}/\bar{R}$. Consequently, the new state vector is: $\vec{x} = \left[\hat{R}, \alpha\right]^T$.

Let now define an open set $\Omega_C = \left\{\vec{x} : \|\vec{x}\| \ge \frac{R_0}{\bar{R}}\right\}$ and a positive definite matrix P that satisfies

$$\|P\| \le \frac{\bar{R}}{2V\eta}\lambda_{min}(Q)$$

where, as shown in appendix,

$$\eta = \sqrt{4 + \left(\frac{R_0}{\bar{R}} + K_2 + 1 + \frac{\bar{R}}{V}\right)^2}$$

and Q is an arbitrarily chosen symmetric positive matrix.

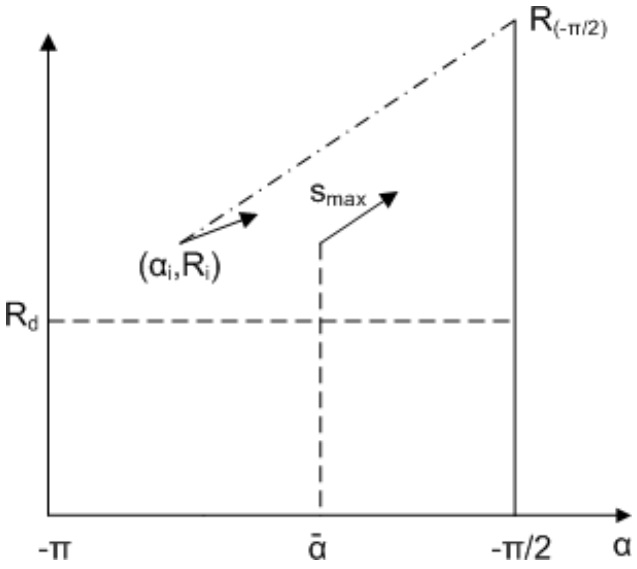

Figure 8. Upper Bound of the Phase Plane

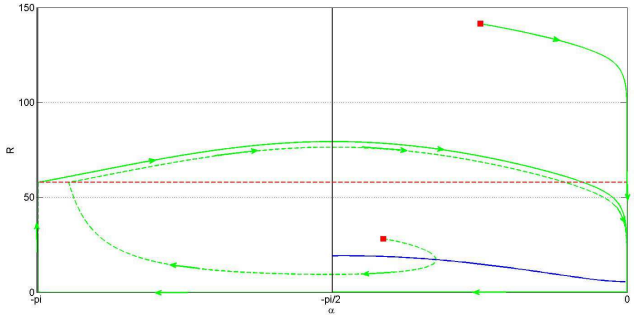

Figure 9. Periodic Orbit

Then, as shown in Appendix A, the proposed guidance law is demonstrated to make the Pursuer-Fixed Target system ultimately bounded (see Fig. 10).

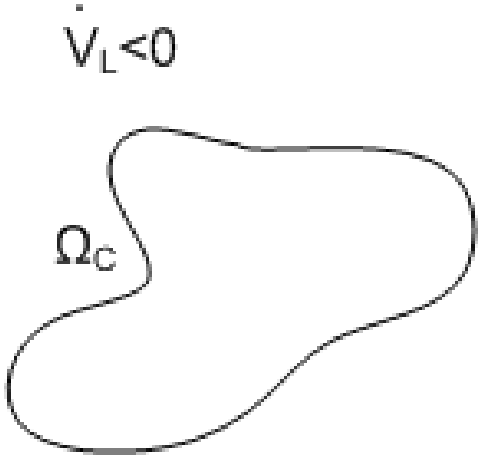

Figure 10. Ultimate boundedness for a Fixed Target

For a moving target it is possible to define a subset $\Omega_\epsilon = \{\vec{x} : \|\vec{x}\| \geq \epsilon\}$, where ϵ is defined in eq. (49). In this way, it is easy to verify that for $\vec{x} \in \Omega_C \cap \Omega_\epsilon$ and

$$\|P\| < \frac{\bar{R}}{2V\eta}\lambda_{min}(Q) \tag{26}$$

an ultimate boundedness stability proof can be derived also for a moving Target.

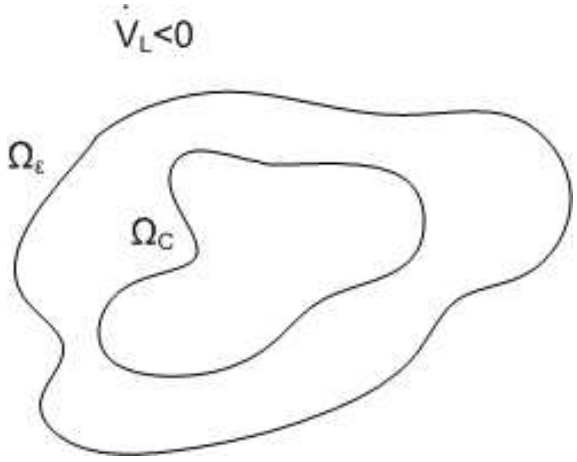

Figure 11. Ultimate boundedness for a Moving Target

Now, considering that $\bar{R}$ can be chosen arbitrarily, matrix P can be chosen consequently.

V. Target Velocity Estimation

In order to compute the guidance law, the knowledge of position and velocity vectors of both the UAV and the ground target is necessary. Position and velocity measurements of the UAV are available from on-board sensors (like a GPS receiver); in this context the position of the target is assumed to be transmitted from ground, while the target velocity is assumed to be unknown. This is mainly due to limit the data-link bandwidth.

The availability of position and velocity information allows for the determination of the parameters used in the computation of the guidance law according to the following relationships:

$$\vec{R} = [x_T - x, y_T - y]^T, R = \left\|\vec{R}\right\|$$

$$\tan(\sigma) = \frac{x_T - x}{y_T - y}$$

$$\vec{V}_G = [\dot{x}, \dot{y}]^T, \vec{V}_T = [\dot{x}_T, \dot{y}_T]^T, \vec{V}_R = \vec{V}_T - \vec{V}_G$$

where $\vec{V}_R$ indicates the target-UAV relative velocity; moreover it can be easily verified that the following expression holds

$$\dot{R} = \frac{\vec{R} \cdot \vec{V}_R}{\|\vec{R}\|}$$

Hence, a filter capable to provide an estimate of the target velocity, together with a smoothed target position information, is needed on-board.

Many filters proposed for this task exist in literature based on variations of Kalman filters (EKF, Unscented, Particle filters, etc.): unfortunately the robustness of the estimation process remains usually a critical problem. Here a simple filter structure is given: its derivation is partially based on the idea of the fast estimator described in Ref.[14]

The filter has to estimate the North and East components of target position and velocity: due to the fact that North and East coordinates are de-coupled, only one channel of the filter is described here, the other one being similar.

The mathematical model of the process to be observed is:

$$\begin{cases} \dot{x}_T = u \\ y = x_T \end{cases} \tag{27}$$

where u denotes the target unknown North velocity, x_T is the target North position, y is the measurement received on-board. The proposed filter is illustrated in Fig. 12 where the hat over the variables indicate the corresponding estimated values. $R(s)$ is a transfer function to be selected in order to make the filter estimation process convergent.

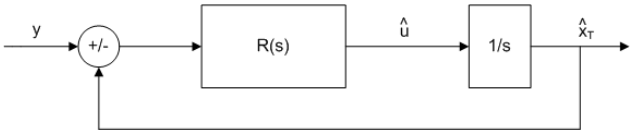

Figure 12. Target velocity estimation scheme

The updating equations of the filter, expressed in the s-domain, are:

$$\hat{x}_T(s) = \frac{R(s)\frac{1}{s}}{1 + R(s)\frac{1}{s}} y(s) \tag{28}$$

$$\hat{u}(s) = \frac{R(s)}{1 + R(s)\frac{1}{s}} y(s) \tag{29}$$

and the velocity estimation error can be expressed by

$$u(s) - \hat{u}(s) = G(s)u(s) \tag{30}$$

where

$$G(s) = 1 - \frac{R(s)}{s + R(s)} \tag{31}$$

By choosing a first order stable transfer function of the type

$$R(s) = \frac{k}{s+c} \tag{32}$$

with k and c positive constants, it results that the filter is stable and the velocity estimation error is bounded.

In particular, by selecting $k = \frac{c^2}{4}$, the filter is a second order system with two coinciding poles. An error estimation bound is given by (see the appendix for the derivation of the results and for the definition of $\mathcal{L}_1$ and $\mathcal{L}_\infty$ norms):

$$\|u - \hat{u}\|_{\mathcal{L}_\infty} \leq \|e_{u0}\|_{\mathcal{L}_\infty} + \|G(s)\|_{\mathcal{L}_1} \|u\|_{\mathcal{L}_\infty} \tag{33}$$

with $e_{u0}(t)$ being the free response of the system $G(s)$ to the initial estimation errors.

Because of the limited speed of the target, it is

$$\|u\|_{\mathcal{L}_\infty} \leq u_{max}$$

hence, from (33), by substuting the results in appendix, it holds

$$\|u - \hat{u}\|_{\mathcal{L}_\infty} \leq M + 2u_{max} \tag{34}$$

with

$$M = \frac{2}{c} B e^{\frac{e_{u0}(0)}{B} - 1}$$

$$B = \|\dot{e}_{u0}(0) + \tfrac{c}{2} e_{u0}(0)\|$$

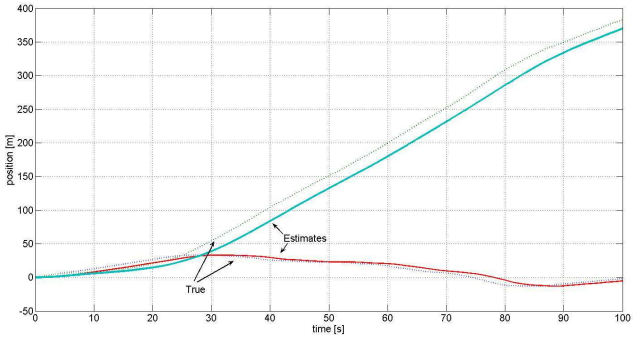

Figure 13. Target position estimation

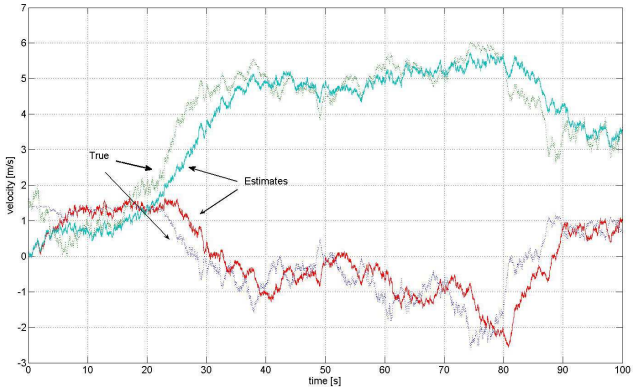

Figure 14. Target velocity estimation

Figures 13 and 14 show the estimated target position and velocity data obtained by the proposed filter under the hypotheses that the target is moving according to a band-limited white noise-like North and East accelerations.

VI. Simulation Results

In this section several simulations results are presented in order to test the effectiveness of the guidance law presented in section III. In these simulations the velocity of the UAV is considered constant at 10 m/s while, when the wind effect is considered, it has a constant from West-direction and a constant speed equal to 3 m/s. The gains used in the guidance law are: $C = 3.6057$, $R_0 = 57.8112$ and $K_2 = 5$. Three different cases are simulated: fixed target, target moving with constant heading, target moving with variable heading; each case is simulated with and without wind.

A. Fixed Target

In this first subsection the target is considered fixed at the origin of the reference frame and two different simulations are presented: the first one with no wind effect while the second with a constant wind. The initial position of the UAV is (100,100) meters with the initial UAV heading pointing to North-East direction. The simulation lasts 100 s.

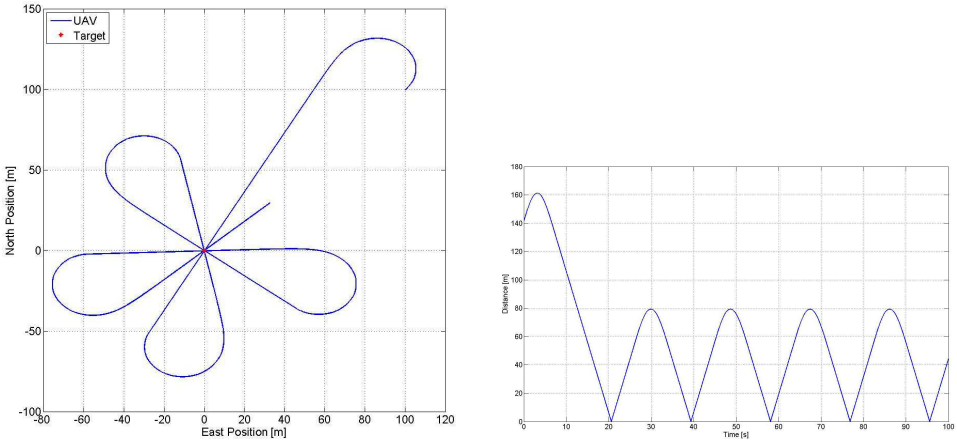

(a) Trajectories of UAV with no Wind Effect (b) Distance UAV-Target with No Wind Effect

Figure 15. Fixed Target and No Wind Effect

In Fig. 15 and 16 (case a) the continuous line represents the trajectories of the UAV. In Fig. 15 no wind effect are considered and the main characteristic of the designed guidance law is highlighted: the UAV is able to always pass over the target. In Fig. 16 the trajectory of the UAV in presence of wind effect are shown. In this case the UAV is also able to pass over the target but with a different trajectory.

These considerations are also documented in Fig. 15 and 16 (case b) where in both cases the distance between the UAV and the target goes periodically to zero. The only slight difference that can be seen between the two figures is the period of interceptions. In presence of wind effects the period is longer.

B. Target Moving along a Straight-line

In this case the target is supposed to move toward North along a straight-line trajectory. However, the speed of the target is variable but always slower than the UAV cruise airspeed. In particular the target's profile velocity is shown in Fig. 17 where, again, from 70 to 250 s the target is considered fixed. It can be seen that the target speed is less than 7 m/s. As in the previous case, the simulations are presented with and without wind effect and the simulated time interval here is 250 seconds.

The trajectoriy of the UAV and the target in the no wind case are represented by, respectively, the continuous line and the dashed line in Fig. 18. In both cases, according to the behavior of the guidance law, the UAV is able to track the target. Moreover, when the target is fixed the UAV flies over the pursuer continuously. The different trajectories created by the guidance law are due to the presence of the wind.

Without the wind effect the trajectory in similar to a constant oscillation around the position of the target until it stops (see Fig. 18). After the first overflight of the target, the UAV remains for some time inside the R_0 circle defined by the guidance law with an increasing relative distance: this explains why the trajectory exhibits a going-away UAV movement during this phase. By observing Fig. 19 it can be seen that

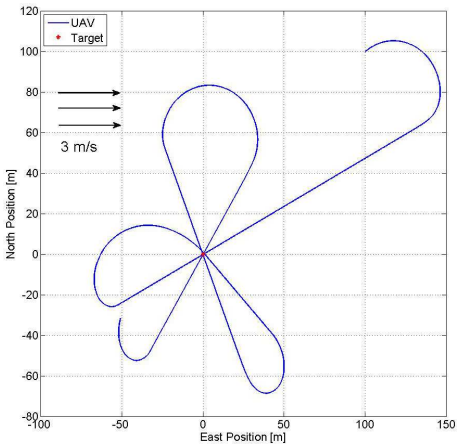

(a) Trajectories of UAV with constant Wind Effect

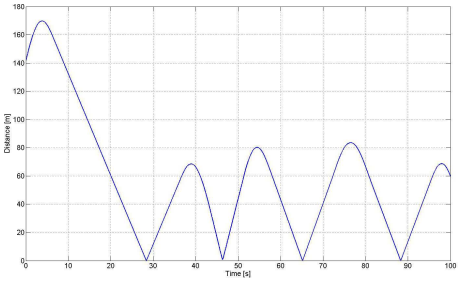

(b) Distance UAV-Target with constant Wind Effect

Figure 16. Fixed Target and Wind Effect

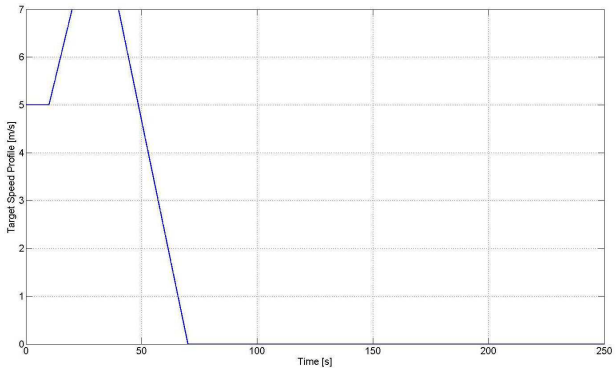

Figure 17. Target Velocity Profile

the UAV, due to the presence and the direction of the wind that reduce the speed of the air-vehicle, points toward the target by remaining behind. However, also in this case, the UAV starts to loiter around the final point reached by the target.

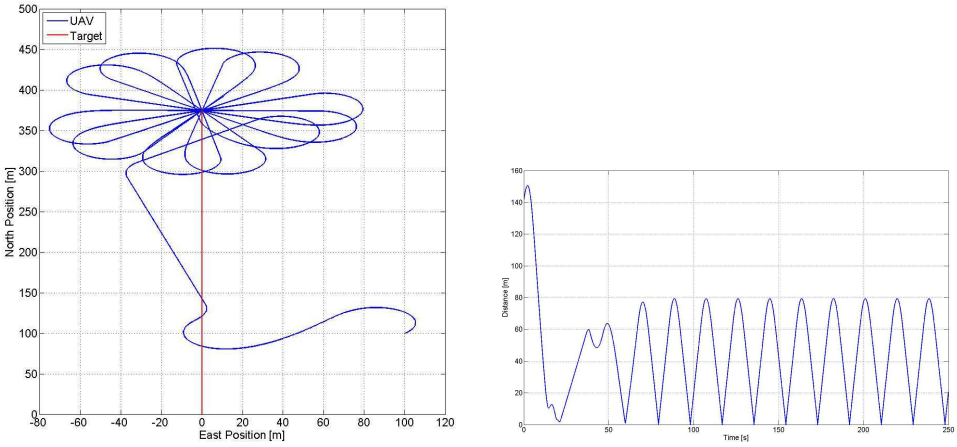

(a) Trajectories of UAV with no wind effect

(b) Distance with no wind effect

Figure 18. Moving Target with no wind effect

Figure 18 (case b) shows the distance between the target and the UAV during the simulation. In this figure the oscillatory motion is shown in the first 50 seconds where the distance between the target and the UAV never goes to zero. Once the target stops, the distance goes, again, periodically to zero. Figure 19 (case b) shows how the UAV intercepts the first time the target at around 50 seconds, avoiding the oscillation motion. Once the UAV reaches the target it starts to loiter around the target as it is shown in the previous case.

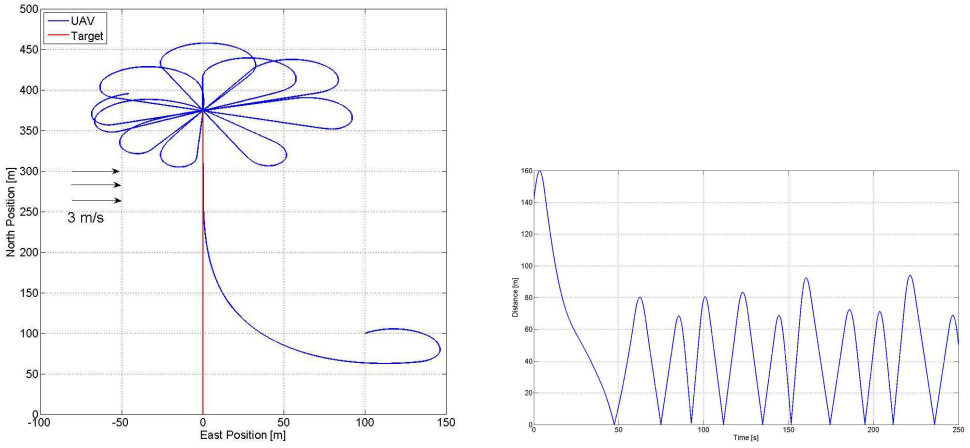

(a) Trajectories of UAV with constant wind effect

(b) Distance UAV-Target with constant wind effect

Figure 19. Moving Target with constant wind effect

C. Circular Path Target Motion

In order to complete the simulations of the proposed guidance law, a circular trajectory is supposed to be followed by the target. The aim of this simulation is to test the guidance law when the target is completing a bend trajectory. In this case the velocity of the target is supposed to be constant at 5 m/s, with a constant lateral acceleration equal to 0.05 m/s^2 and, as in the previous cases, wind and no-wind simulations are shown.

The initial position of the UAV is (100,0) with North-East initial heading angle. The target is initially placed at the origin (0,0) of the reference frame. The simulation lasts 100 seconds. In Fig. 20 the continuous line represents the UAV trajectory while the dashed line is the target trajectory. Both in Fig. 20 (without wind) and in Fig. 21 (constant wind) is shown that the UAV is able to intercept the target and starts to loiter around while it is keeping moving.

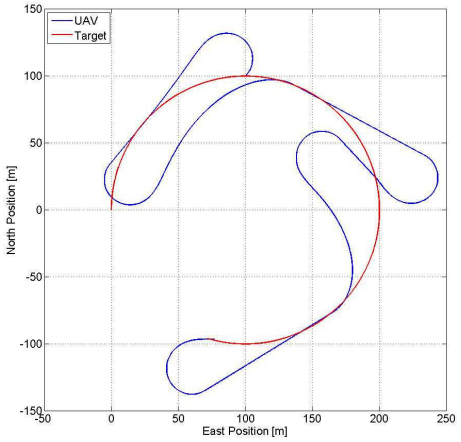

(a) Trajectories of UAV with no wind effect

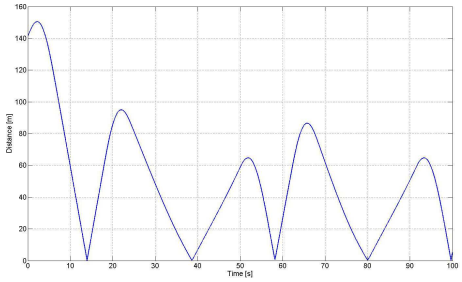

(b) Distance with no wind effect

Figure 20. Moving Circular Target

Figure 20 (case b) shows that the distance between the UAV and the target goes to zero. The periodic behavior cited in the previous case is confirmed here where the maximum distance between the target and the UAV is around 60 m. The target is intercepted at constant periods of 25 seconds each.

Figure 21 (case b) shows that the UAV is able to reach the target but, due to the presence of the wind, the trajectory created by the guidance law is not periodic anymore.

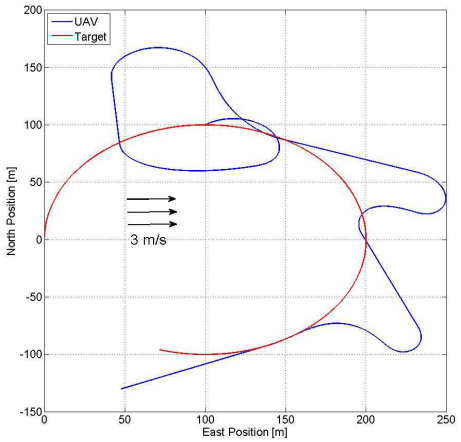

(a) Trajectories of UAV with constant wind effect

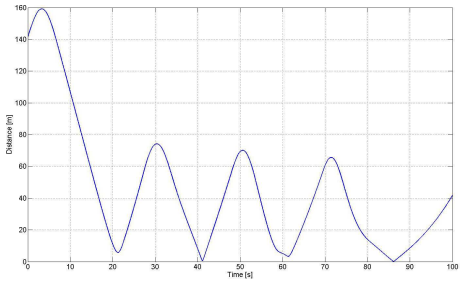

(b) Distance with constant wind effect

Figure 21. Moving Circular Target

D. Comments

In all the cases analyzed in this section (*A, B, C*) the guidance designed law has the expected behavior. In particular the aim to create a guidance law able to continuously fly over the target is reached. Moreover, fig. 18 and fig. 20 show that the guidance law ensures that the distance goes to zero also when the target is moving.

VII. HIL Ardupilot Simulation

The proposed guidance law described in sec. III has been implemented on the electronic board ArduPilot-Mega (APM). One of the main features of this micro-controller is the open source firmware which can be easily modified by any user. In particular, the APM 2.12 source code has been changed to ensure a Hardware In the Loop (HIL) target tracking simulation. The setup is sketched in fig. 22.

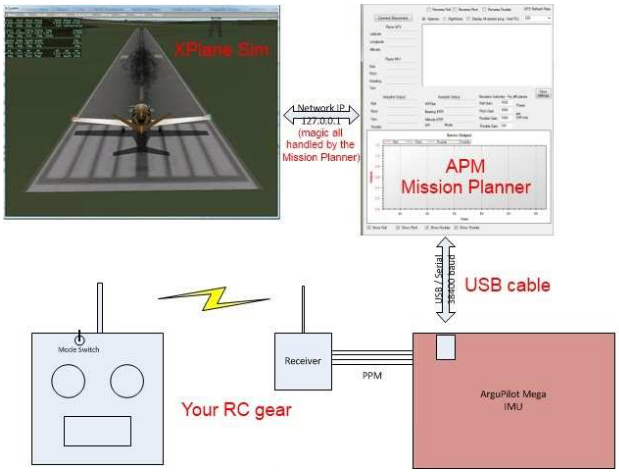

Figure 22. Setup of HIL simulation

The Six Degrees of Freedom (6DoF) flight simulator chosen for HIL simulation is X-Plane and, in order to have a more realistic simulation, the Radio-Controlled (RC) airplane of the University of Bologna, an Eagle FPV model (see fig. 23), has been modeled in X-Plane software through the plane maker program. The characteristics of the plane are described in table 2.

Figure 23. Eagle FPV RC Model

Together with the APM source code, ArduPilot-Mega offers the chance to use the Mission Planner (known also as ground station) which serves as a bridge between the board and X-Plane software. The ground station reads the data coming from the flight simulator and sends it, through the serial port, to the APM. At the same time it sends the servo outputs calculated by the autopilot to X-Plane.

The results of two different simulations are presented. In the first one a moving target has been simulated while in the second simulation a fixed target position has been chosen in order to highlight the main characteristic of the proposed guidance law to ensure a continuous over-loitering on it. Both the simulations have been carried out with these parameters:

	Wing	Horizontal Stabilizer	Vertical Stabilizers
Span	1.66 $[m]$	0.53 $[m]$	0.17 $[m]$
Mean Aerodynamic Chord	0.23 $[m]$	0.16 $[m]$	0.2 $[ft]$
Airfoil	NACA 4412	NACA 0012	NACA 0012
Incidence	0.0 [deg]	8.5 [deg]	–
Deflection	±40 [deg]	±40 [deg]	±40 [deg]

Table 2. University of Bologna UAV Geometric Characteristics

- Aircraft Cruise Speed V = 15 [m/s];
- Wind Speed 3 [m/s];
- Wind Direction 30;
- Desired radius 100 [m]
- C = 15, $K_2 = 0.3$.

A. HIL Moving Target

In order to simulate a target tracking, a trajectory has been completed by a car and its data (position, speed and heading) sampled by a GPS receiver at 0.3 Hz. All these data have been provided and processed on ArduPilot-Mega; then it has been possible to simulate the RC airplane behaving as an UAV following a moving car.

Figure 24 shows the 3D trajectory of the UAV. The yellow pointers represent the data sampled by the GPS receiver on-board the car while the red line is the trajectory completed by the UAV. It is also significant to monitor attitude, altitude and the distance between the UAV and the moving target (Fig. 25).

As can be seen the UAV follows the target and its attitude shows a bounded roll angle and a stable pitch which can be also seen by the altitude profile. The distance plot shows sometimes values over 500 [m] but this is due to the speed reached by the ground target. It is obvious that if the target goes faster than the UAV distance increases but it drops quickly around 150 [m] when the car decreases its speed.

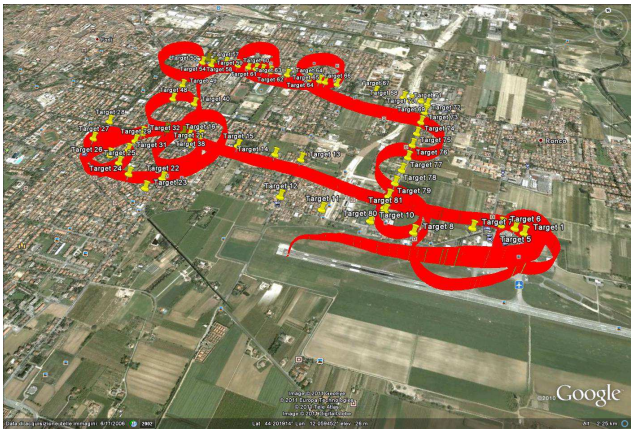

Figure 24. 3D HIL trajectories

B. HIL Fixed Target

In this simulation a fixed target has been supposedly placed near Forli' Airport. As can be seen a continuous over-loitering of the fixed point is performed by the UAV. As in the previous subsection the roll angle remains

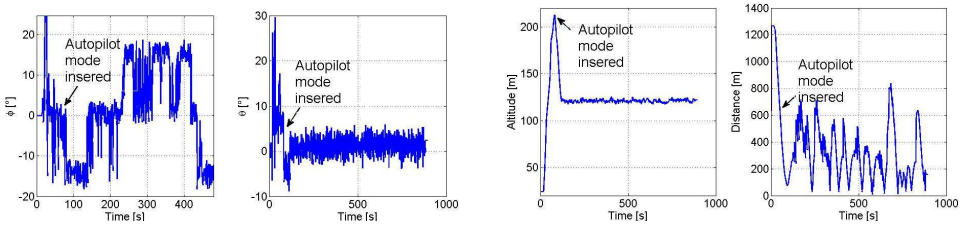

(a) Roll and Pitch angles (b) Height and Distance

Figure 25. UAV Data

bounded; the same for the pitch angle and altitude. It is important to see how the distance reduces close to zero cyclically (Fig. 27).

Figure 26. 3D HIL trajectories

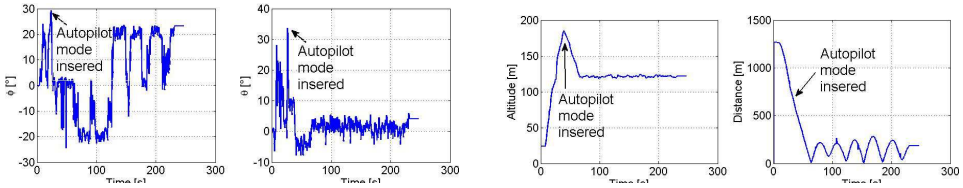

(a) Roll and Pitch angles (b) Height and Distance

Figure 27. UAV Data

VIII. Conclusion

A new guidance law for a fixed-wing Unmanned Aerial Vehicle (UAV) with surveillance and/or tracking purposes has been presented. It allows for a continue overflying of the target whether it is fixed or when it moves, without the knowledge of a preplanned path. The guidance law fulfills the requirements of flight mechanics constraints such as the constancy of airspeed and bounded lateral acceleration. In case of no wind and moving target, a proof of stability and criteria for the development of the parameters of the guidance law have been given. An assessment of the performances by means of software simulations and hardware-in-the-loop tests have shown that of the presented law successfully reaches its goal, even in presence of wind, with a minimum computation burden due to its relative low complexity.

Appendix

A. Ultimate Boundedness Stability

1. *Fixed Target*

Considering eq. (12) it is possible to present the tracking problem as:

$$\dot{\vec{x}} = f(\vec{x}) \tag{35}$$

where $\vec{x} = [\hat{R}, \alpha]^T$ represents the new state vector.

Now, by adding and subtracting the term $A_0\vec{x}$ in eq. (35), where A_0 is the following Hurwitz matrix:

$$A_0 = \begin{bmatrix} 0 & -\frac{1}{\bar{R}} \\ \frac{1}{\bar{R}} & -1 \end{bmatrix} \tag{36}$$

it becomes

$$\dot{\vec{x}} = A_0\vec{x} + f(\vec{x}) - A_0\vec{x} \tag{37}$$

In order to prove the boundedness of the proposed guidance law, an initial state where $R \geq R_0$ can be considered or, equivalently, $\hat{R} \geq \frac{R_0}{\bar{R}}$. Hence, the value of $K_1(R, \dot{R}) = C$.

Moreover, consider the open set $\Omega_C = \left\{\vec{x} : \|\vec{x}\| \geq \frac{R_0}{\bar{R}}\right\}$.

By defining $\Gamma(\vec{x}) = f(\vec{x}) - A_0\vec{x}$ and considering C equal to $\frac{V^2}{\bar{R}}$, it results

$$\Gamma(\vec{x}) = \frac{V}{\bar{R}}\begin{bmatrix} -\cos(\alpha) + \alpha \\ \frac{\sin(\alpha)}{\hat{R}} - \arctan(K_2\alpha) - \hat{R} + \frac{\bar{R}\alpha}{V} \end{bmatrix} \tag{38}$$

The square of the norm of $\Gamma(\vec{x})$ results:

$$\|\Gamma(\vec{x})\|^2 = \left(\frac{V}{\bar{R}}\right)^2\left[(-\cos(\alpha)+\alpha)^2 + \left(\frac{\sin(\alpha)}{\hat{R}} - \arctan(K_2\alpha) - \hat{R} + \frac{\bar{R}\alpha}{V}\right)^2\right] <$$

$$\leq \left(\frac{V}{\bar{R}}\right)^2\left[(|\alpha| + |\alpha|)^2 + \left(\frac{|\alpha|}{\hat{R}} + K_2|\alpha| + |\alpha| + \frac{\bar{R}|\alpha|}{V}\right)^2\right] \leq$$

$$\leq \left(\frac{V|\alpha|}{\bar{R}}\right)^2\left[(2)^2 + \left(\frac{1}{\hat{R}} + K_2 + 1 + \frac{\bar{R}}{V}\right)^2\right]$$

This last inequality holds because:

- $-\cos(\alpha) \leq |\alpha|$;
- $-\arctan(K_2\alpha) \leq K_2|\alpha|$;
- $\frac{\sin(\alpha)}{\hat{R}} \leq \frac{|\alpha|}{\hat{R}}$;
- $-\hat{R} \leq |\alpha|$ because $\hat{R} \geq 0$.

Now, by defining

$$\eta^2 = 4 + \left(\frac{R_0}{\bar{R}} + K_2 + 1 + \frac{\bar{R}}{V}\right)^2 \tag{39}$$

it results that:

$$\|\Gamma(\vec{x})\|^2 < \left(\frac{V}{\bar{R}}|\alpha|\eta\right)^2 \tag{40}$$

Considering $\|\vec{x}\|^2 = |\alpha|^2 + \left|\hat{R}\right|^2$ and that $|\alpha| \leq \|\vec{x}\|$ the following inequality holds:

$$\|\Gamma(\vec{x})\| < \frac{V}{\bar{R}} \|\vec{x}\| \eta \tag{41}$$

If one defines a Lyapunov function

$$V_L = \vec{x}^T P \vec{x} \tag{42}$$

where P is a symmetric positive definite matrix, its time derivative results:

$$\dot{V}_L = \dot{\vec{x}}^T P \vec{x} + \vec{x}^T P \dot{\vec{x}} = \vec{x}^T \left({A_0}^T P + P A_0 \right) \vec{x} + 2\Gamma(\vec{x})^T P \vec{x} \tag{43}$$

The matrix P can be chosen in order to verify ${A_0}^T P + P A_0 = -Q$, with Q symmetric positive definite matrix arbitrarily chosen; hence eq. (43) becomes:

$$\dot{V}_L = \dot{\vec{x}}^T P \vec{x} + \vec{x}^T P \dot{\vec{x}} < -\left(\lambda_{min}(Q) - \frac{2V\eta}{\bar{R}} \|P\| \right) \|\vec{x}\|^2$$

Now if

$$\|P\| < \frac{\bar{R}}{2V\eta} \lambda_{min}(Q) \tag{44}$$

the Lyapunov time derivative function is a decreasing function: hence, for any $\vec{x} \in \Omega_C$ the ultimate boundedness of the proposed guidance law is derived.

2. Moving Target

Starting from eq. (2), which describes the tracking kinematic problem, it is possible to make the same variable changes described in sec. IV: $(\alpha = \sigma - \chi)$ and $(\hat{R} = \frac{R}{\bar{R}})$. Assuming, as before, $R \geq R_0$, the tracking problem becomes

$$\begin{cases} \dot{\hat{R}} = \frac{1}{\bar{R}} \left(V_T \cos(\alpha + \chi - \chi_T) - V \cos(\alpha) \right) \\ \dot{\alpha} = \frac{1}{\bar{R}} \left(-\frac{V_T \sin(\alpha + \chi - \chi_T)}{\hat{R}} + \frac{V \sin(\alpha)}{\hat{R}} - V \arctan(K_2 \alpha) \right) \end{cases} \tag{45}$$

where, as in the fixed target case, the wind effect is not considered $(V = V_G)$.
By posing $\chi_R = \chi - \chi_T$, model (45) can be written as:

$$\begin{cases} \dot{\hat{R}} = -\frac{V}{\bar{R}} \cos(\alpha) + \frac{V_T}{\bar{R}} \cos(\alpha + \chi_R) \\ \dot{\alpha} = \frac{V}{\bar{R}} \left(\frac{\sin(\alpha)}{\hat{R}} - \arctan(K_2 \alpha) \right) - \frac{V_T}{\hat{R}\bar{R}} \sin(\alpha + \chi_R) \end{cases} \tag{46}$$

The state space model (46) can be represented by

$$\dot{\vec{x}} = f(\vec{x}) + g(\vec{x}) \tag{47}$$

where $g(\vec{x})$ is:

$$g(\vec{x}) = \frac{V_T}{\bar{R}} \begin{bmatrix} \cos(\alpha + \chi_R) \\ -\frac{\sin(\alpha + \chi_R)}{\hat{R}} \end{bmatrix} \tag{48}$$

Now, according to the procedure used in the fixed target section, it is possible to define

$$\gamma(\vec{x}) = \Gamma(\vec{x}) + g(\vec{x})$$

where $\Gamma(\vec{x})$ is defined by eq. (38)
Hence is

$$\|\gamma(\vec{x})\| = \|\Gamma(\vec{x})\| + \|g(\vec{x})\| \leq$$
$$\leq \frac{V}{R}\|\vec{x}\|\eta + \frac{V_T}{R}\sqrt{(\cos(\alpha+\chi_R))^2 + (\frac{\sin(\alpha+\chi_R)}{\hat{R}})^2} \leq$$
$$\leq \frac{V}{R}\|\vec{x}\|\eta + \frac{V_T}{R}\sqrt{\frac{\hat{R}^2+1}{\hat{R}^2}} =$$
$$= \frac{V}{R}\|\vec{x}\|\eta + \frac{V_T}{R}\sqrt{\hat{R}^2+1} =$$
$$= \frac{V}{R}\|\vec{x}\|\eta + V_T\sqrt{\frac{1}{R^2}+\frac{1}{R^2}}$$

then

$$\|\gamma(\vec{x})\| \leq \frac{V}{R}\|\vec{x}\|\eta + V_T\sqrt{\frac{1}{R^2}+\frac{1}{R_0^2}}$$

By considering a Lyapunov function similar to the one in eq. (42), its time derivative results:

$$\dot{V}_L \leq -\|\vec{x}\|\left\{\left[\lambda_{min}(Q) - \frac{2V\eta}{R}\|P\|\right]\|\vec{x}\| - 2V_{Tmax}\sqrt{\frac{1}{R^2}+\frac{1}{R_0^2}}\|P\|\right\}$$

Consequently if

$$\|\vec{x}\| \geq \epsilon$$

where

$$\epsilon = \frac{2V_{Tmax}\sqrt{1+\frac{\bar{R}}{R_0^2}}\|P\|}{\bar{R}\lambda_{min}(Q) - 2V\eta\|P\|} \tag{49}$$

and eq. (44) holds, the Lyapunov time derivative of eq. (42) is negative definite in the set:

$$\vec{x} \in \Omega_C \cap \{\|\vec{x}\| \geq \epsilon\} \tag{50}$$

B. Bound for Velocity Estimation Error

The definitions of $\mathcal{L}_1$ and $\mathcal{L}_\infty$ norms are:

$$\|u\|_{\mathcal{L}_\infty} = \sup_{0\leq\tau\leq t}|u(\tau)|$$

$$\|G(s)\|_{\mathcal{L}_1} = \int_0^\infty |g(\tau)|\,d\tau$$

where $u = u(t)$ is a time-continuous signal, $g(t)$ is the impulse response of a linear system, $G(s)$ is the Laplace transform of $g(t)$.

If the Input-Output model of a system in the s-domain is

$$y(s) = G(s)u(s) \tag{51}$$

then the time response $y(t)$ is

$$y(t) = y_0(t) + \int_0^t g(\tau)u(t-\tau)d\tau \tag{52}$$

where $y_0(t)$ is the free response to the initial conditions.

Hence, it holds

$$\|y\|_{\mathcal{L}_\infty} \leq \|y_0\|_{\mathcal{L}_\infty} + \left\|\int_0^t g(\tau)u(t-\tau)d\tau\right\|_{\mathcal{L}_\infty} \tag{53}$$

and, from (53),

$$\|y\|_{\mathcal{L}_\infty} \leq \|y_0\|_{\mathcal{L}_\infty} + \|G(s)\|_{\mathcal{L}_1}\|u\|_{\mathcal{L}_\infty} \tag{54}$$

If

$$G(s) = \frac{s(s+c)}{s(s+c)+k} \tag{55}$$

by selecting $k = \frac{c^2}{4}$, $c > 0$, it holds

$$G(s) = s\frac{(s+c)}{(s+\frac{c}{2})^2} \tag{56}$$

whose impulse response $g(t)$ is

$$g(t) = \delta(t) - \frac{c^2}{4} t e^{-\frac{c}{2}t} \tag{57}$$

where $\delta(t)$ is the Dirac impulse.
After simples passages the following expression can be obtained

$$\|G(s)\|_{\mathcal{L}_1} = \int_0^\infty |g(\tau)|\, d\tau = 2$$

Moreover, in this case the free response can be computed after some algebra and gives:

$$y_0(t) = (y_0(0) + Bt)e^{-\frac{c}{2}t} \tag{58}$$

with

$$B = \dot{y}_0(0) + \frac{c}{2} y_0(0)$$

$|y_0(t)|$ admits a maximum for $t > 0$ whose value is $M = \frac{2}{c}|B|e^{\frac{y_0(0)}{B}-1}$. Hence

$$\|y_0\|_{\mathcal{L}_\infty} = M \tag{59}$$

References

[1]Wang, I., Dobrokhodov, V., Kaminer, I., and Jones, K., "On Vision-Based Tracking and Motion Estimation for Moving Targets Using Small UAVs," *Proceedings of Guidance Navigation and Control Conference*, AIAA, San Francisco, CA, USA, 2005.

[2]Dobrokhodov, V., Kaminer, I., Jones, K., and Ghabcheloo, R., "Vision-Based Tracking and Motion Estimation for Moving Targets Using Small UAVs," *Proceedings of Guidance Navigation and Control Conference*, AIAA, Key Stone, CO, USA, 2006.

[3]Dobrokhodov, V., Kaminer, I., Jones, K., Kistios., I., Cao, C., Ma, L., Hovakimyan, N., and Wosley, C., "Rapid Motion Estimation of a target Moving with Time-Varying Velocity," *Proceedings of Guidance Navigation and Control Conference*, AIAA, Hilton Head, SC, USA, 2007.

[4]Nelson, D., Barber, B., McLain, T., and Bear, W., "Vector Field Path Following for Miniature AirVehicle," *IEEE Transaction on Robotics*, Vol. 23, No. 3, 2007.

[5]Lawreance, D., Frew, E., and Pisano, W., "Lyapunov Vector Field for Autonomous UAV Flight Control," *Proceedings of Guidance and Navigation Control Conference*, AIAA, Hilton Head, SC, USA, 2007, pp. 6317 – 6339.

[6]Regina, N. and Zanzi, M., "UAV Guidance Law for target Tracking along a Constrained Bow-Shaped Trajectory based on Lyapunov Vector Field," *Proceedings of Symposioum on Aerospace Control Automation*, IFAC, Nara, Japan, 2010.

[7]Park, S., Deyst, J., and How, J., "A New NonLinear Guidance Logic for Trajectory Tracking," *Proceedings of Guidance and Navigation and Control Conference*, AIAA, Providence, Rhode Island, 2004.

[8]Park, S., Deyst, J., and How, J., "Performance and Lyapunov Stability of a Nonlinear Path-Following Guidance Method," *Journal of Guidance,Control and Dynamics*, Vol. 30, No. 6, 2007.

[9]Gates, D., "NonLinear Path Following Method," *Journal of Guidance, Control and Dynamics*, Vol. 33, No. 2, 2010.

[10]Lin, C., *Modern Navigation Guidance and Control Processing Vol.2*, Prentice Hall,Upper Saddle River (NJ), 1991.

[11]Zennaro, M. and Sengupta, R., "Strategies of Path-Planning for a UAV to Track a Ground Vehicle," *Proceedings of the AINS Conference*, AINS, Bologna, IT, 2003.

[12]Lalish, E., Morgansen, K., and Tsukamaki, T., "Oscillatory Control for Constant-Speed Unicycle-Type Vehicles," *Proceedings of 46th IEEE Conference on Decision and Control*, IEEE, New Orleans, LA, USA, 2007, pp. 5246 – 5251.

[13]Regina, N. and Zanzi, M., "UAV Guidance Law for Ground-based Target Trajectory Tracking and Loitering," *Proceedings of Aerospace Conference*, AIAA/IEEE, Big Sky, MT, USA, 2011.

[14]Ma, L., Cao, C., Hovakimyan, N., Dobrokhodov, V., and Kaminer, I., "Adaptive Vision-Based Guidance Law with Guaranteed Performace Bounds," *Journal of Guidance, Control and Dynamics*, Vol. 33, No. 3, 2010.

[15]Regina, N. and Zanzi, M., "2D Tracking and OverFlight of a Target by means of NonLinear Guidance Law for UAV," *Proceedings of Aerospace Conference*, AIAA/IEEE, Big Sky, MT, USA, 2009.

[16]Dobrokhodov, V., Kaminer, I., Jones, K., and Ghabcheloo, R., "Vision-Based Tracking and Motion Estimation for Moving Targets Using Unmanned Air Vehicles," *Journal of Guidance, Control and Dynamics*, Vol. 31, No. 4, 2008.

[17]ZuWhan, K. and R.Sengupta, "Target Detection and Position Likelihood Using an Aerial Image Sensor," *Proceedings of International Conference on Robotics and Automation*, ICRA/IEEE, Pasadena, CA, USA, 2008.

[18]Bertuccelli, L. and How, J., "Search for dynamic Targets with uncertain probability maps," *Proceedings of American Control Conference*, IEEE, Minneapolis, MI, USA, 2006.

[19]Guo, W., Zhao, Y., and Capozzi, B., "Optimal Unmanned Aerial Vehicle Flights for Seeability and Endurance in Winds," *Journal of Aircraft*, Vol. 48, No. 1, 2011.

[20]Khalil, H., *Nonlinear System*, Prentice Hall, 2002.

[21]Raymer, D., *Aircraft Design: a conceptual approach*, AIAA Education Series, 1999.